

FABRICATION OF A COST-EFFECTIVE MEMS-BASED PIEZORESISTIVE CANTILEVER SENSOR FOR GAIT MOVEMENT ANALYSIS

A.F.M. Anuar^{1,2}, S. Saadon^{1,2*}, Y. Wahab^{1,2}, H. Fazmir^{1,2}, M.Z. Zainol^{1,2}, S. Johari², M. Mazalan^{1,2}

¹Advanced Multi-Diciplinary MEMS-Based Integrated NCER Centre of Excellent (AMBIENCE)

²School of Microelectronic Engineering (SoME), Universiti Malaysia Perlis, Malaysia

*E-mail: saadonsalem@yahoo.com

(Received 28 December 2015; accepted 24 July 2016)

Abstract

Gait analysis measurement is a method used to access and identify gait events and the measurements of motion parameters involving the lower part of the body. This significant method is widely used in rehabilitation, sports, and health diagnostics for improving the quality of life. However, it is not a routine practice due to costs involved in creating and using gait labs. Alternatively, inertial sensors such as microcantilever accelerometer can be used in the development of cheap and wearable gait analysis systems. Human stride segmentation measurement based on a micro-accelerometer cantilever is used in the study of the lower limb movement patterns that include walking, jumping and running, as well as the measurements of the motion parameters. A complete system consisting of a fabricated sensor, a Wheatstone bridge circuit, and a signal amplifier tailored for real-time stride analysis measurement is proposed. A novel fabrication method for an accelerometer sensor using laser micromachining is introduced in order to develop a simple way for realizing sensor formation. This study allows us to optimize the requirements of hard-mask and fabrication process steps by reductions of 30% and 25% respectively. In the general framework, this research activity is focused towards the development of a piezoresistive cantilever formation using laser micromachining for fast fabrication development of a real life gait and stride segmentation measurement application.

Keywords: MEMS, accelerometer, micro cantilever, piezoresistor, polysilicon, silicon, KrF laser, micromachining, gait analysis

Introduction

Gait analysis is a very important procedure in assessing and improving many quality of life indicators. It is widely used in rehabilitation, sports, and health diagnostics. Gait analysis is the study of lower limb movement patterns and involves the identification of gait events and the measurements of kinetics and kinematics parameters. These include, for example, toe-off, landing, stance, swing, displacement, speed, velocity, acceleration, force, and pressure (Bakar, 2013). Gait cycle can be determined as a period of walking composed of a single step of the right and left foot. Every gait cycle consists of the unique characteristics of a person's movement, which contributes to gait signature. The length of gait cycle for every person is different. In general, the average walking speed of a person is roughly at one gait cycle per second. Figure 1 shows the stride pattern in the suspensory ligament of a walking human as measured using an industrial accelerometer.

The realization of an accelerometer sensor is needed in evaluating the biometric properties of human gait. Microfabrication technology is the key of functional integration and miniaturization of electronics system. Micro-Electro-Mechanical System (MEMS) technology has grown rapidly during the previous two decades, especially in commercial applications of sensors and actuators (Vinod Jain, 2013). MEMS can produce the small integration devices which involve a combination of sensors, actuators, electronic and mechanical elements on a common silicon substrate through microfabrication technology. In order to fabricate a complex three-dimensional structure without a mask, micromachining with laser ablation is the best option. In 1982, polymer-like materials were investigated by researchers using Excimer laser radiation (Kawamura, Toyoda, & Namba, 1982). Depending on the processing materials, each laser pulse has its own merits and demerits.

MEMS based mass-beam structure has been proven as an outstanding Microfabrication platform for extremely sensitive devices such as biochemical and environmental sensors. In terms of mechanics and biomechanics, micro-mechanical sensors such as the microcantilever is suited to study the analysis of human movement activities and environmental sensing.

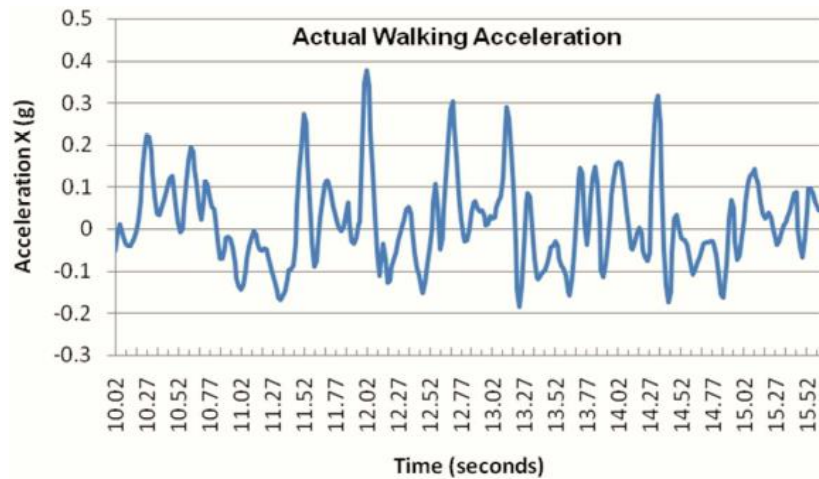


Figure 1: Stride pattern in the suspensory ligament of a walking human measured using an industrial accelerometer (Slaughter & Hilbert, 2009).

Experimental Section

At the first stage, poly-silicon is deposited by a Low-Pressure-Chemical-Vapor-Deposition (LPCVD) process to create thin layer of piezo-resistive layer. At high temperatures (in the range of 600 - 650 °C) and vacuum conditions, silane (SiH₄) will decompose and silicon can be deposited on the heated surface (Xiao, 2001). A 100nm thick film of poly-silicon were deposited on SiO₂ passivation thin film. The overall experiments were conducted by deposition, doping, and annealing to obtain uniform poly-silicon grains (Boutchich, Ziouche, Godts, & Leclercq, 2002).

In the conventional experimental procedures, piezo-resistive microcantilever fabrication consists of multiple wet and dry etch processes. To the best of our tools and knowledge, the RapidX-250 series of laser micromachining is used in assisting the pattern structure for the device. The accuracy and fast factors in MEMS piezo-resistive cantilever development are important. The basic resistance of a rectangular shaped section of poly-resistor film is given by Equation 1, where ρ is resistivity of poly-silicon sheet (Su, 2004).

$$R = \rho \frac{l}{wt} \tag{1}$$

The 248nm wavelength is a deep laser commonly used in semiconductor industrial manufacturing. The RapidX-250 series of KrF Excimer micromachining is used in this research as part of an Excimer laser system. The most important aspects provided by laser pulsed micromachining include good quality at high resolutions, high precision, high process speeds, low thermal damage and applicability to many materials (Holmes, Pedder, & Boehlen, 2006). Besides, it also allows for highly flexible Computer Numerical Control (CNC) programming depending on prototyping shapes, and requires few processing steps, smaller cleanroom facilities and fewer hazardous human substances. The system used in this research is shown in Figure 2, consisting of mechanical parts and X-Y stages orientation of laser beam delivery system controlled by an user friendly software (Wahab & Bakar, 2011).

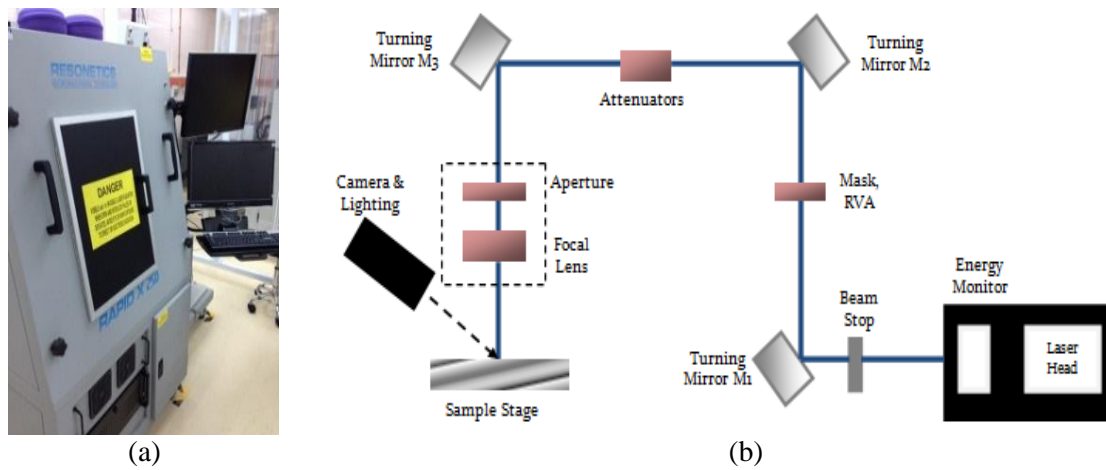


Figure 2: KrF Excimer laser micromachining system; (a) Physical structure of Resonetics laser micromachining, (b) Laser beam circulation and internal hardware system.

The frequency of the laser beam emission is sufficiently energetic to break the chemical bonds of most materials (Holmes, Pedder, & Boehlen, 2006). As shown in Figure 3, laser pulses are bombarded on the silicon surface. In this section, photochemical process occurs and laser energy absorbed by the silicon surface. Thus, heat is generated and leads to the photo-thermal process. The unique characteristic of the Excimer laser with 248nm optical wavelength is that it provides high resolution ($\sim 1 \mu\text{m}$) features on the target surface, while the etching process on a silicon substrate at a power of 15mJ will create 0.1 μm to 2 μm average depth into the sample (Su, 2004). The piezo-resistor resistant value is dependent on the shapes which constructed by laser automation. The structure of silicon microcantilever development is also assisted by the Excimer laser micromachining. In this research, silicon substrate with the thickness of 30 μm is prepared for the microcantilever development. Laser energy at 15 mJ and 0.5mm of RVA are used on the sample. The beam size needs to be considered because it will affect the total parameter of the design.

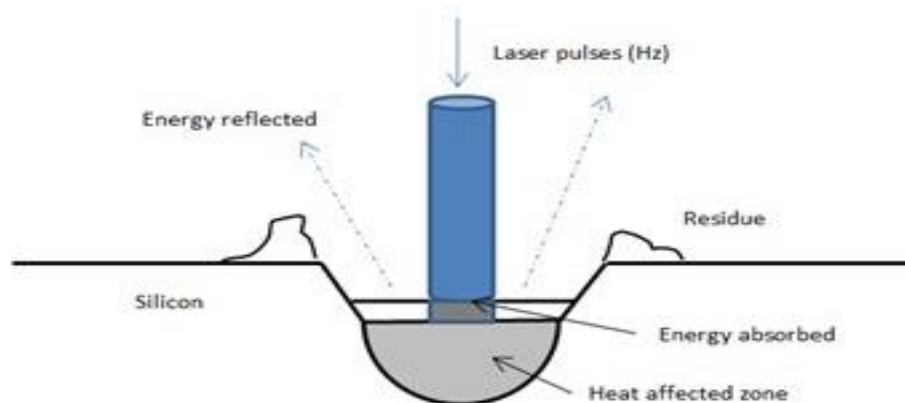


Figure 3: Interaction between laser and silicon material (Anuar et al., 2014).

In Figure 4, we show a comparison of the overall steps regarding piezo-resistor fabrication by using conventional and laser micromachining technique. The packaged procedures in conventional needs multiple photolithography and wet etch process to create resistor structure as desired. In conventional, hard mask is required to produce resistor shapes. On the other hand, hard masks are eliminated in micromachining steps. At first, the mask pattern structure is designed in computer-aided software and run automatically by the automated system. Figure (d) shows both techniques as illustrations of the resistor final structure with a 3-dimensional view.

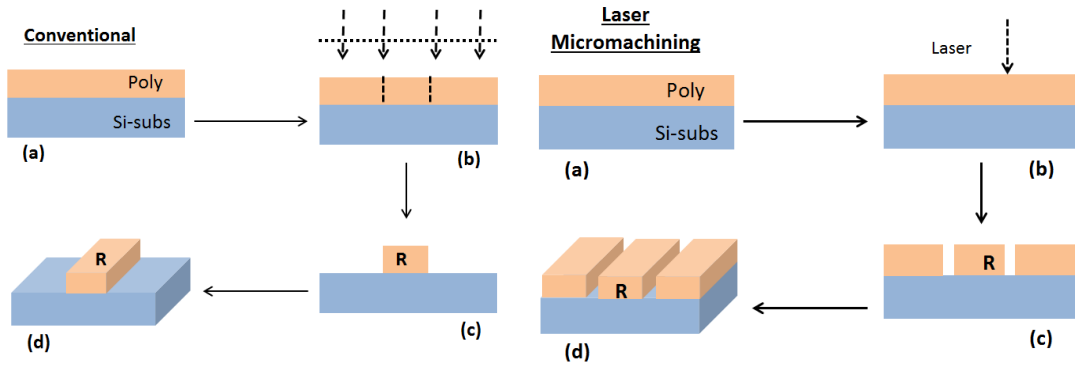


Figure 4: Conventional and laser micromachining technique for resistor formation.

The piezoresistive effect is the change in resistivity of a material caused by the application of a stress. The well-known phenomenon is quite large in semiconductors devices (Singh, Ngo, Seng, Neo, & Mok, 2002). Figure 5 shows the four resistors connected in the Wheatstone bridge configuration. One of the resistors is the piezoresistor, which is implemented in microcantilever structure to sense the applied stress. The others resistor has a fixed value and is integrated on the printed circuit board. From the schematic, the resistance change of the piezoresistors will always be the change of the current value for the entire circuit. When the cantilever beam bends downward and upward, it causes tensile stress on the piezoresistor surface, changing the electrical value of the entire system.

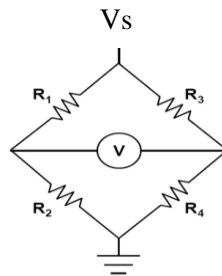


Figure 5: Schematic of Wheatstone bridge circuit; where $R4$ is the piezoresistor in the piezoresistive microcantilever sensor.

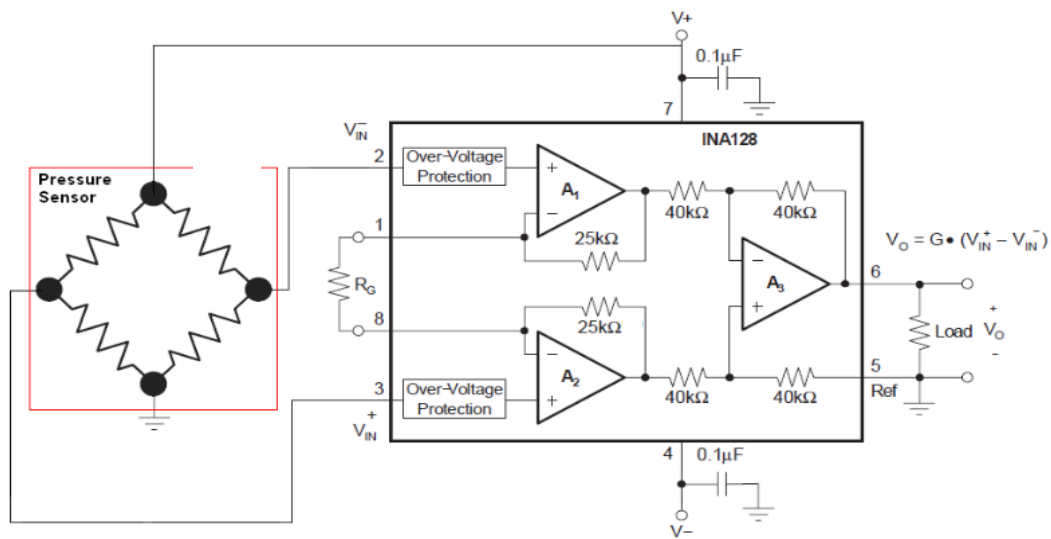


Figure 6: Schematic of Wheatstone bridge circuit and the instrumental amplifier (Wahab, 2009).

The resistance, R of the fabricated piezoresistor can be proven and calculated using Equation 1, where l is the microcantilever length, A is the area of the microcantilever, and ρ is the resistivity ($\Omega\mu\text{m}$) (Madzhi, Khuan, & Ahmad, 2010). An instrumental amplifier is applied to the sensor in order to measure the environmental signals. Input signal from the Wheatstone bridge is amplified using the differential gain of the INA128

amplifier. Figure 6 shows the schematic of the sensor integration which consists of Wheatstone bridge and differential operational-amplifier circuit with the multiply gain of 50.

$$V_o = V_{in} \left(\frac{R_4}{R_3 + R_4} - \frac{R_2}{R_1 + R_2} \right) A_v \quad (2)$$

If the balancing resistors in bridge circuit are equal i.e. $R_1/R_2 = R_3/R_4$, the output voltage, V_o can be calculated using Equation 2, where $R_3 = R + \Delta R$ and the gain is 50.

Results and Discussion

Silicon Micromachining

Crystalline silicon is a common semiconductor material widely used nowadays for microelectronic fabrications. In order to find the best recipes for Excimer laser ablation of silicon materials, a set of experiments with different parameters was conducted. The main parameter investigated in this research is laser energy (mJ) which is laser beam energy level that are supplied to form laser beam. The number of laser pulses in second is a part of important criteria for the Excimer laser experiment. The maximum number of laser pulses provide by the RapidX-250 laser micromachining is 300 pulses. The number of pulses will determine the laser line pattern either in gross or smooth line. Besides, etch rate in $\mu\text{m}/\text{shot}$ is defined as average etched depth by each laser shot. The other parameter required in this research is the laser beam size aspect ratio, which is defined as Rectangular Variable Aperture (RVA) in millimeters.

Etch Depth

The micromachining patterns on a silicon substrate were observed using high power microscope (HPM) with various lens magnification. The tested patterns with different pulse frequencies on a single line were successfully imaged on the sample shown in Figure 7. The experiments were carried out with unchanged parameters, unless a different pulse repetition on the same line is required. Figure 7(a) illustrates the 9.08 μm of the etch depth with 30 times of pulse passes on a single surface. The etch depth for every sample is inversely proportional to increasing the number of laser passes. This result can be concluded by the range of energy beam laser is reduce to certain degree length of sample. Besides, the existence of the debris from the process will cover the drain pattern, thus reducing the efficiency of laser beam energy to penetrate to another depth layer.

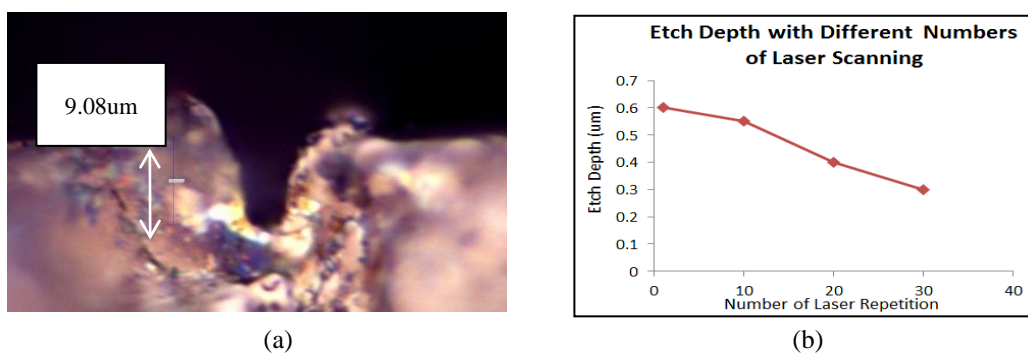


Figure 7: Etch rate characteristics; (a) Etch depth for 30 times lasers scanning, (b) Relations between number of laser scanning and etch depth.

- Rectangular Variable Aperture (RVA)

The size of laser ablation illustration can be obtained by comparing the width geometries of the laser sizes. Figure 8 compares 0.5mm, 1.0mm and 2.0mm of RVA with constant energy supplied. The double beam width size of RVAs is shown in Figure 8(a) and Figure 8(b). This result can be used to conclude that the laser beam size controlled by the RVA mechanism will produce 70 μm of pattern beam width on the sample by 1.0mm RVA size.

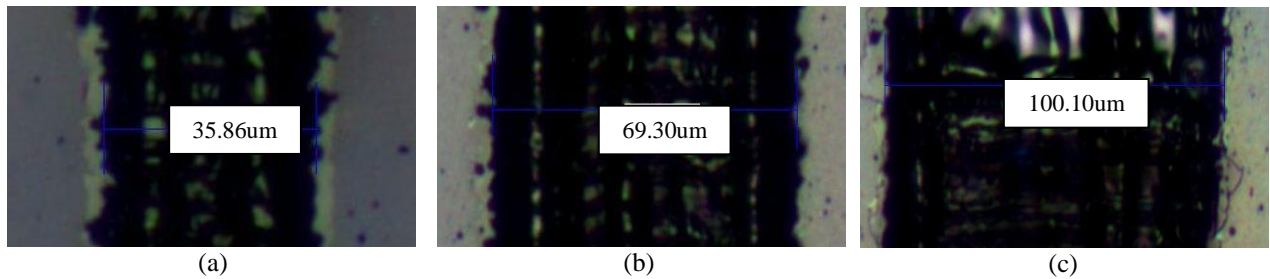


Figure 8: Laser ablation by differences RVA; (a) 0.5mm; (b) 1.0mm; (c) 2.0mm.

- *Power*

Energy level is important in the design of structures which have varying effects on depth and surface profiles. The precise desired pattern can be achieved by ensuring the sufficient power needs by the target. The range of the KrF Excimer laser micromachining laser energy can be varied from 1mJ to 18mJ. The surface morphology of the sample tested using laser power at 12mJ, 15mJ and 18mJ are shown in Figure 9. Based on these results, it can be concluded that 15mJ is the suitable energy for laser to fire up the structure on the silicon substrate. The smoothness of the top view profile for this parameter is suitable in structuring and cutting the piezoresistor and cantilever shapes for the sensor fabrication.

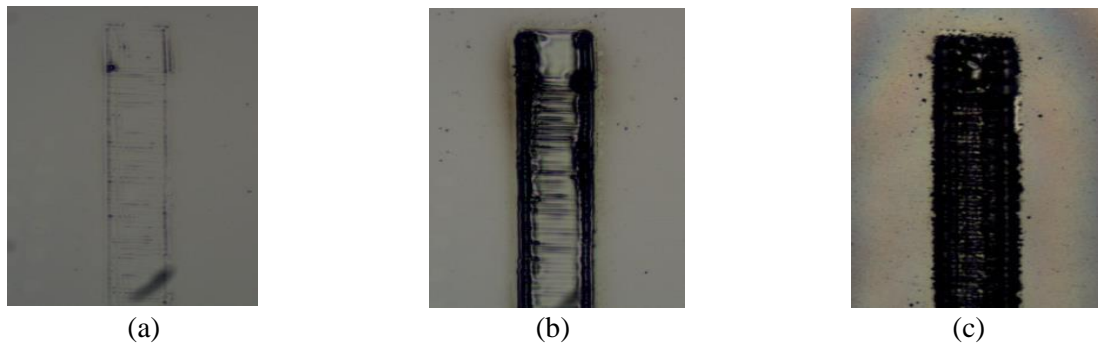


Figure 9: Surface morphology with difference energy level; (a) 12mJ; (b) 15mJ; (c) 18mJ.

- *Pulse Number*

The smoothness and planarization of the silicon surface is also affected by the pulse number of the laser. In this research, we found that using a low number of laser pulse will provide high roughness on the depth of firing structure. Thus, a zig-zag pattern will be likely produce by a laser beam. Figure 10 shows the top surface of the sample with different number of laser pulse. The variables of pulse number can be adjusted in the range of 1 to 300 pulses. The approximately parameter as Figure 10(b) is the ideal pattern, because the rectangular beam structure is not too far or close. The increasing pulse number will produce high volume of silicon debris which will overlap back to the drain pattern. This activity will cover the thickness for every shot laser on the sample.

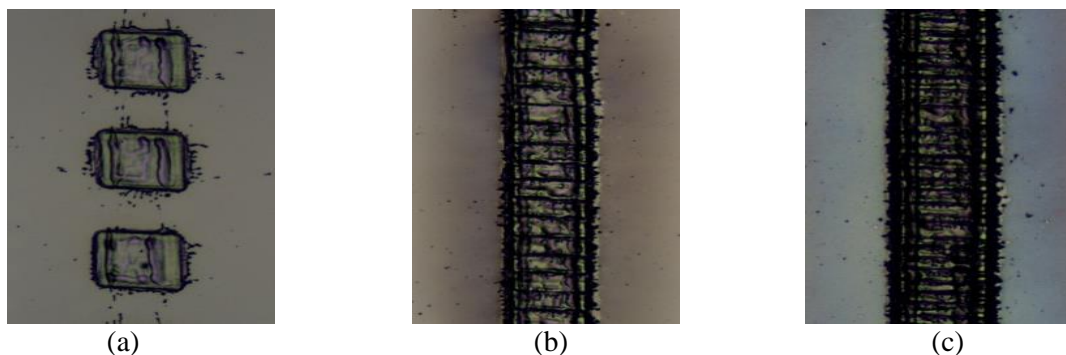


Figure 10: Differences in pulse number; (a) 10 pulses; (b) 50 pulses; (c) 100 pulses.

Poly-resistor Thin Film Deposition and Formation

Polysilicon deposition is normally a low-pressure chemical vapor deposition (LPCVD) process, which is deposited in a furnace with a vacuum system. At high temperatures in the range of 600 - 650 °C and vacuum condition, silane (SiH_4) will decompose and silicon can be deposited on the heated surface (Xiao, 2001). A 100nm thin film of polysilicon was deposited by LPCVD on SiO_2 passivation thin film. The deposition was performed in a LPCVD furnace with 80 sccm of SiH_4 gas and 600 °C of process temperature. A total of 10 minutes processing time was required in order to create the 100 nm average thickness of polysilicon thin film layer. Annealing was performed at a temperature of 900 °C in the furnace with nitrogen gas for 30 minutes. Nitrogen gas is needed because it acts as a purging gas in order to avoid the possibility of oxidation and nitridation on polysilicon film during annealing process (Jing, Yunfei, Jinling, Longjuan, & Fuhua, 2009). High resistivity is achieved by deposition of undoped semiconductor LPCVD polysilicon. Then the diffusion process proceeds with liquid boron source (BBr_3) to obtain a heavily doped poly-silicon film. A liquid source was chosen for diffusion process to assist in producing a high concentration doping level. The overall experiments were conducted by deposition, doping, and annealing to obtain uniform poly-silicon grains (Boutchich et al., 2002). Illustrations for surface roughness and uniformity of polysilicon grains have been obtained by atomic force microscopy (AFM), as shown in Figure 11.

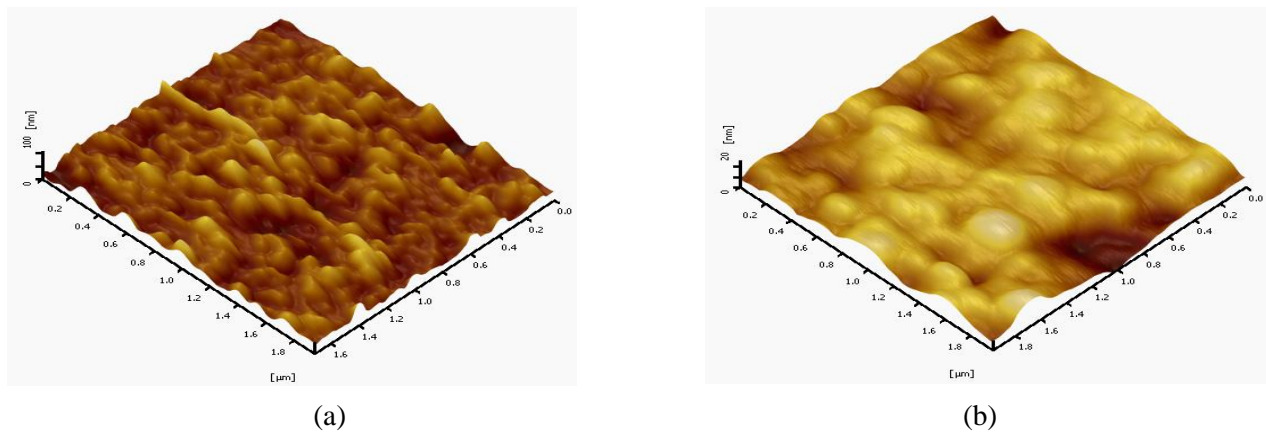


Figure 11: The AFM results for polysilicon surface roughness and uniformity. (a) Before annealing; (b) After annealing at 900 °C for 30 minutes.

KrF Excimer micromachining is used in the patterning of polysilicon thin film to produce various shapes of poly-resistor. Figure 12 shows a section of the physical structure of the patterned poly-resistor. As discussed before, the parameters include scanning passes of laser pulses, which are set to five in order to totally isolate the resistor region from others.

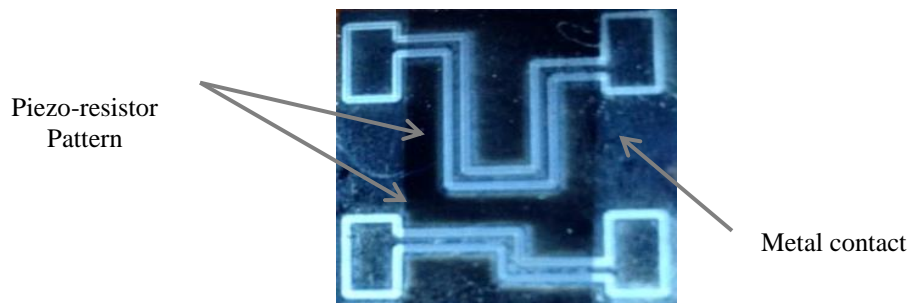
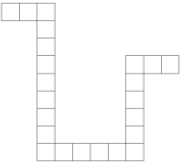
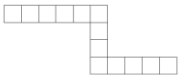


Figure 12: Top view of the fabricated poly-resistor.

A layer of oxide passivation of 87 nm was grown on silicon substrate. Subsequently, 108 nm of polysilicon was deposited as the resistor material. The diffusivity of the boron in the polysilicon grain and boundaries is measured by four-point probe and semiconductor parametric analyzer (SPA). The low resistance polysilicon sheet is revealed after the removal of borosilicate glass by 10% diluted HF. Table 1 shows the illustration and parameters involved in the resistor formation process. 21 and 12 total squares are designed and fabricated, thus producing resistances of 303.52 Ω and 210.14 Ω , respectively. However, the differences of

the resistance per unit square between these two values can be considered high in error tolerances. The uniformity and doping concentration of polysilicon layer are the factors most affected by these values.

Table 1: Poly-Resistor layout and parameters.

| Poly-Resistor Layout | Total Square | Measurement Value (Ω) | Resistance per Square (Ω/\square) |
|---|--------------|--------------------------------|--|
|  | 21 | 303.52 | 14.45 |
|  | 12 | 210.14 | 17.51 |

Microcantilever Sensor Formation

The cantilever dimension was designed in AutoCAD with 1000um x 350um of length and width, respectively. The 30um of the sample thickness is prepared first by using wet etch process. In Figure 13, a microcantilever structure has been produced by 15 times of laser beam passes. The experimental result shows the dimension of microcantilever of 950um x 300um for the length and width respectively. It is demonstrated that the features of pulse etching depth can be defined as 0.5um per scan for silicon substrate. Low power and small beam size are used in the formation of microcantilever because of the lower edge roughness and heat radiation on the side of the line. These factors may interfere with the characteristics of the deposited material on the substrate if the microcantilever is to be used as sensor. However, the overall shapes and pattern are formed as desired in patterning the piezo-resistor and microcantilever shapes which both are integrated as inertia sensor.

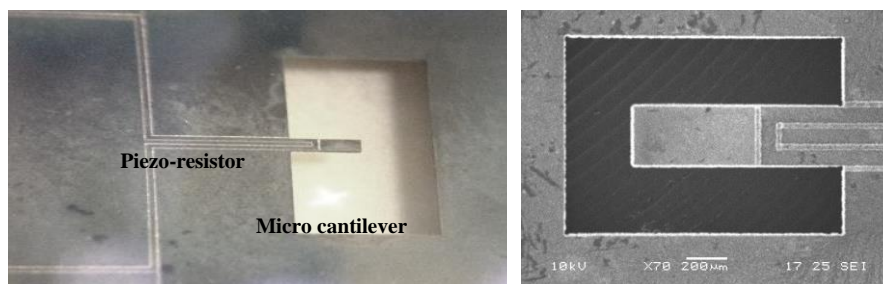


Figure 13: Image of fabricated sensor, by 950x300x 30um for the length, width and thickness respectively.

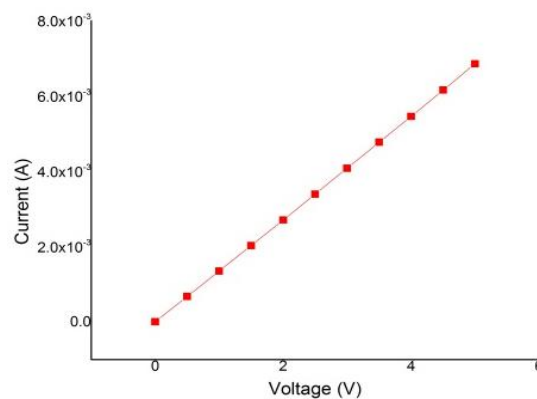


Figure 14: I-V characteristics of the piezo-resistor.

The current-voltage characteristic of the fabricated piezo-resistors is measured using semiconductor parametric analyzer at room temperature. The resistor current characteristic is fairly linear with the voltage range. The average resistance given by Figure 14 is 670 Ω , thus proved that the resistor has behaved as theoretical expected. The sheet resistance of the zero-stress value covered by a unit square is 4.5 Ω/\square . In

order to apply a force to the cantilever beam, the custom-made printed circuit board is designed to bond with the sensor by thin gold wire through wire bonding process.

System Integration

Since a single on-chip piezoresistor was diffused using Boron with the resistance value of 670Ω , a resistance value within the range of 670Ω was chosen for the other balancing resistor in the external Wheatstone bridge circuit. If all the legs have equal resistance value, the bridge is balanced; hence, zero output voltage can be obtained. Table 2 shows the difference output voltage for the Wheatstone bridge balancing circuit, where $R4$ is the artificial piezoresistive micro cantilever.

The balanced arm bridge result is achieved when all the resistances are changed to null value, thus producing zero output voltage. From Table 1, it can be seen that the output voltage from the bridge is almost equal for null bridge condition when $R4$ equals 670Ω . The initial setup for the sensor experiment should be zero in order to analyze different conditions during responses. Table 2 also shows the outcome from a comparative study between experimental and theoretical results of the circuit balancing legs. It can be observed that the measured output voltage and the theoretical values have an average difference of 4.3%.

Table 2: Measurement results of output voltage and variable resistor, $R4$ for the Wheatstone bridge balancing circuit.

| Balancing Resistor $R1, R2, R3$ (Ω) | Variable Resistor $R4$ (Ω) | Calculated Output voltage (V) | Measured Output voltage (V) |
|---|-------------------------------------|----------------------------------|--------------------------------|
| 670 | 600 | -0.138 | -0.153 |
| 670 | 610 | -0.117 | -0.120 |
| 670 | 630 | -0.077 | -0.078 |
| 670 | 650 | -0.038 | -0.054 |
| 670 | 670 | 0 | 0.192 |
| 670 | 690 | 0.038 | 0.022 |
| 670 | 710 | 0.072 | 0.070 |
| 670 | 730 | 0.107 | 0.125 |
| 670 | 750 | 0.141 | 0.155 |

The previous experimental outcome verified the performance of the sensor using a Wheatstone bridge circuit. A possible range around 670Ω has been chosen as the variable resistance value range, as it meets the piezoresistance value when in zero-deflection condition. A complete set of electro-dynamic vibration system, including a shaker, is used to generate vibration input to the sensor. Microcantilever is fixed on a base and vibration is produced by the shaker so that the beam will vibrate as illustrated in Figure 15. An oscilloscope is used to measure the cantilever beam characteristic in terms of voltage change due to the piezoresistive effect. Different acceleration and force magnitudes were generated by the vibration system in order to study the basic properties of the fabricated cantilever. In the second experiment, we recorded the ΔV oscillation peak-to-peak voltage (V_{pp}), which represents the microcantilever vibration change due to the different force given to the base. Figure 17 shows the graph of the sensor response in terms of output voltage as a function of force magnitudes. By monitoring the output voltage that we received from the response, the maximum acceleration force that the piezoresistive sensor can withstand is around 0.8 g, where $g = 9.81 \text{ m/s}^2$.

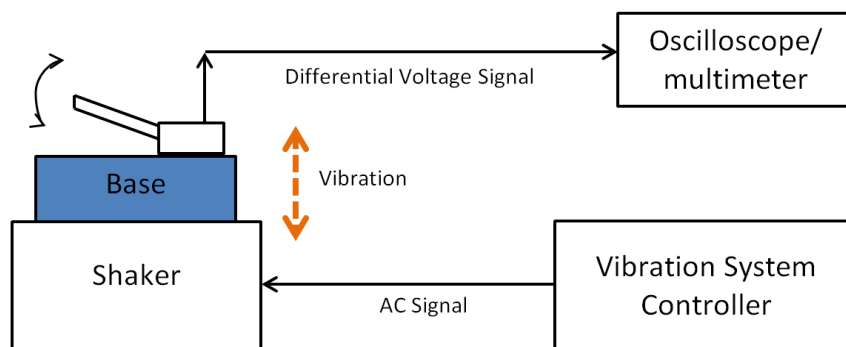


Figure 15: Vibration system configuration.

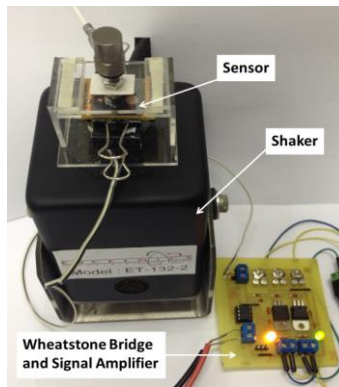


Figure 16: Experimental setup to measure sensor response to the applied vibration.

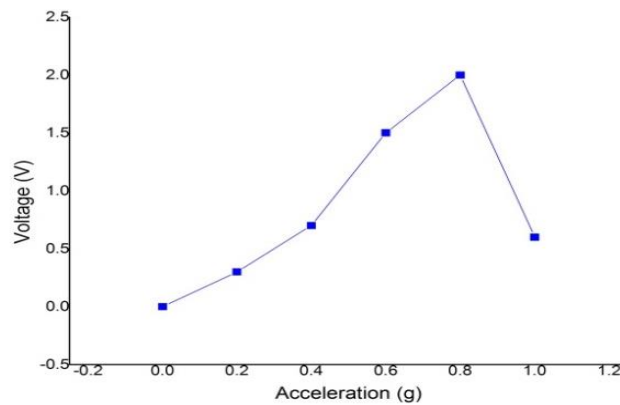


Figure 17: Measured sensor responses to acceleration, ranging from 0g to 1g.

Verification of Human Stride Motion Principle

In gait analysis identification, the dynamic responses for walking and running have been studied using the fabricated sensor. The properties of these two motions are shown in Figure 18. In theory the cycle starts at the point where the acceleration is zero. In practice the zero points are rarely found. Thus the starting point is decided to be a negative value which is followed by a positive value which shown in Figure 18(b). After the first and endpoints are detected, the estimation of the cycle length can be measure. Via observation of the voltage and time in the cycle length, the acceleration data for gait motion is analyzed. It shows that the number of cycle groups in running motion is twice compared to walking in a single second period. As shown in the voltage axis, the magnitude of voltage is also high for a running subject. For a realistic comparison, we already know that in the running phase the swinging of the knee is accelerating fast and proportional with the body force given to the ground. The evaluation of these characteristic, especially for the voltage or force, can be proven by Newton’s second law equation, which states that an object is equal to the mass with multiplied by the acceleration vector.

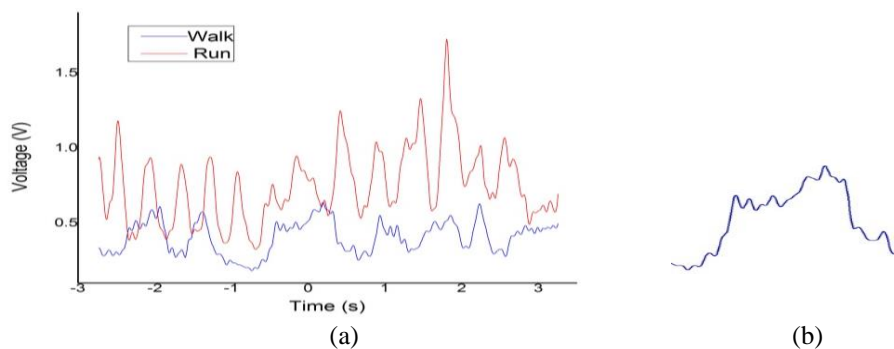


Figure 18: Physical representation of gait activities; (a) Comparison between running and walking movements, (b) Single cycle pattern from the graph.



Figure 19: Placement of fabricated sensor attached on the leg.

Conclusions

We propose a novel method in fabrication of piezoresistive microcantilever by using laser micromachining. The fabricated sensor can be used in applications, especially human gait movement analysis, which require small scale device in operation. We also identified the best steps and features in optimizing the sensor's process steps requires. The measured output voltage from circuit is in close agreement with the calculated values. The presence of force or vibration causes a resistance change in the microcantilever beam, thus generating a signal which is converted to voltage by the Wheatstone bridge and signal amplifier circuit. An electro-dynamic vibration system, including a shaker, is used to generate vibration input to the sensor, and we found that the piezoresistive sensor can tolerate maximum acceleration force of up to 0.8 g with respect to the beam structure designed. The presented results demonstrate that a combination of parameters in laser micromachining, structure dimension and design verification is suitable for structuring the piezoresistive microcantilever sensor. Electrical results for the sensor also showed that the system can function as desired in recognition of the dynamic responses in human strides for walking and running segmentation.

Acknowledgments

It is a pleasure to thank Assoc. Prof. Dr Yufridin Wahab, Dr. Shazlina Johari, Mr. Mazlee Mazalan and research colleague for many fruitful discussions during the research. This work was supported by NCIA using the SNUCOE and N-SILICON grants. All research was carried out at the Advanced Multi-Disciplinary MEMS-Based Integrated NCER Centre of Excellent (AMBIENCE), School of Microelectronic Engineering, Universiti Malaysia Perlis, Perlis, Malaysia.

Author Contributions (ONLY for Research Articles)

Many thanks go to Prof Assoc Dr Yufridin Wahab, Dr Shazlina Johari, Dr Salem Saadon, Mazlee Malazan and research colleagues for many fruitful discussions according to the research topic. This work was supported by NCIA using the SNUCOE, N-SILICON and FRGS 9003:00405 grants. All research was carried out at the Advanced Multi-Disciplinary MEMS-Based Integrated NCER Centre of Excellent (AMBIENCE), School of Microelectronic Engineering, Universiti Malaysia Perlis, Perlis, Malaysia.

Conflicts of Interest

The authors declare no conflict of interest.

References

- Anuar, A. F. M., Wahab, Y., Fazmir, H., Najmi, M., Johari, S., Mazalan, M., Nor, N. I. M., & Md Arshad, M. K. (2014). *KrF Excimer Laser Micromachining of Silicon for Micro- Cantilever Applications*. Proceedings of International Electronic Conference on Sensors and Applications, 1–6.
- Bakar, N. A. (2013). Portable shoe integrated instrumentation for gait analysis measurement using MEMS based devices. (Master dissertation). Retrieved from <http://myto.upm.edu.my/myTO/myto/2/paparthesis/398074.html>
- Boutchich, M., Ziouche, K., Godts, P. & Leclercq, D. (2002). *Characterization of phosphorus and boron heavily doped LPCVD polysilicon films in the temperature range 293-373 K*. *IEEE Electron Device Letters*, 23(3), 139–141.
- Holmes, A. S., Pedder, J. E., & Boehlen, K. L. (2006). *Advanced laser micromachining processes for MEMS and optical applications*. Proceeding SPIE (Society of Photographic Instrumentation Engineers), 6261, 62611E–62611E–9
- Jing, X., L. Yunfei, L., Jinling, Y., Longjuan, T., & Fuhua, Y. (2009). Stress and resistivity controls on in situ boron doped LPCVD polysilicon films for high- Q MEMS applications,” *Journal of Semiconductors*, 30(8).
- Kawamura, Y., Toyoda, K., & Namba, S. (1982). Effective deep ultraviolet photoetching of polymethyl methacrylate by an Excimer laser. *Applied Physics Letters*, 40(5), 374.
- Laser Micromachining Seminar. Retrieved from <http://docslide.us/documents/micro-machining-seminar.html>
- Madzhi, N. K., Khuan, L. Y., & Ahmad, A. (2010). Development of a Low Cost Self-Sensing Piezoresistive Microcantilever Biosensor and Read-Out Circuitry for Measuring Salivary-Amylase Activity,” *Electronic Computer Technology (ICECT), 2010 International Conference*, 9–13
- Singh, R., Ngo, L. L., Seng, H. S., & Mok, F. N. C. (2002). *A Silicon Piezoresistive Pressure Sensor*. The 1st IEEE International Workshop on Electronic Design, Test and Applications (DELTA '02), 181.
- Slaughter, S. C. & Hilbert, C. (2009). *Quantifying and learning human movement characteristics for fall prevention in the elderly using Inertial Measurement Units and Neural Networks*. Proceeding on 2nd International Conference of Education, Research and Innovation Madrid, Spain. 16-18 November. Publisher: IATED.
- Su, J. T. Y. (2004). *A Material System for High Precision Embedded Polymer Resistor*. Proceedings. 9th International Symposium on Advanced Packaging Materials: Processes, Properties and Interfaces, 11, 74–77.
- Vinod Jain, S. V. (2013). Design and Analysis of MEMS Piezoresistive Three layers Microcantilever-based Sensor for Biosensing Applications,” *International Journal Innovative Technology Exploring Engineering*, 2(5).
- Wahab, Y. (2009). *Design and Implementation of MEMS Biomechanical Sensors for Real-Life Measurements of Gait Parameters* (Doctoral dissertation). Retrieved from <http://vuir.vu.edu.au/15499/1/YufridinWahab.pdf>.
- Xiao, H. (2001). *Introduction to Semiconductor Manufacturing Technology*. New Jersey, US: Pearson Education.